Liquid Crystals, Vol. 31, No. 7, July 2004, 895–906

Taylor & Francis
Taylor & Francis Group

Study of smectic elastomer films under uniaxial stress

R. STANNARIUS†‡*, R. KÖHLER†, M. RÖSSLE§ and R. ZENTEL§
†Universität Leipzig, Inst. für Experimentalphysik I, Linnéstr. 5,
D-04103 Leipzig, Germany
‡Otto-von-Guericke-Universität Magdeburg, Inst. für Experimentalphysik,
Universitätsplatz 2, D-39106 Magdeburg, Germany
§Universität Mainz, Inst. für Organische Chemie, Duesbergweg 10–14,
D-55099 Mainz, Germany

(*Received 15 December 2003; accepted 27 February 2004*)

We study the mechanical properties of free-standing films of smectic liquid crystalline elastomers. Macroscopically ordered elastomer films of submicrometer thickness are prepared from freely suspended smectic A polymer films by photo crosslinking. The deformation characteristics depend criticically on the sample composition, in particular on the density of mesogenic side chains at the siloxane backbone. In materials where the siloxane backbone is only partially substituted (dilute systems), a uniaxial stretching of the films in the layer plane is accompanied by a shrinkage of the smectic layers. This layer shrinkage is to only a minor extent achieved by the induction of a molecular tilt. We conclude that the layer compression modulus (enthalpic contribution to elasticity) in such materials is very weak. In materials with a fully substituted backbone (homopolymers), the smectic layer thickness is preserved under uniaxial stress in the layer planes.

1. Introduction

Liquid crystal elastomers (LCEs) combine in a unique way rubber elasticity with anisotropic liquid crystalline properties [1–6]. The growing scientific interest in these materials results primarily from their potential for non-display LC applications in actuators or sensors, but moreover, they are attractive from a general scientific point of view [7–12]. In particular, elastomers in the tilted chiral smectic C* mesophase are of interest because they can exhibit a spontaneous electric polarization, ferro- and piezo-electricity [2, 13–19]. The structure, dynamics and mechanical properties of LCEs have been explored with various experimental methods [19–37].

As a basis for electro-mechanical applications, a comprehensive understanding of the elastic properties and of the coupling mechanisms between electrical field and mechanical deformations is needed. The goal of this study is the investigation of mechanical deformations of macroscopically ordered ('single crystal') smectic LC elastomers under uniaxial stress. Previously, smectic elastomers under stress have been investigated by Finkelmann *et al*. [27–29]. In their samples, it was found that the large layer compression modulus in the smectic A phase prevents the compression of the smectic structure normal to the layers. Consequently, oriented smectic A samples that are stretched uniaxially in the smectic layer plane can contract exclusively in the layer plane, in the direction perpendicular to the stretching axis. This is in contrast to the behaviour of isotropic rubbers which contract in all directions normal to the stretching axis. In addition, measurements of the elastic moduli of ordered elastomer samples have been reported by Weilepp *et al*. [30]. These measurements have shown that the elastic modulus of these materials is independent of the stress direction at temperatures where the material is in the isotropic phase, whereas the elasticity becomes highly anisotropic when the sample is cooled to the smectic A phase. Due to the additional influence of the smectic layer compression modulus, the storage modulus increases significantly in measurements where stress is applied normal to the smectic layers.

Elastic measurements on a random side chain copolymer, consisting of a siloxane backbone and attached mesogenic groups and crosslinker units, have been performed previously [31–33]. In these experiments, thin ordered polymer films were inflated to spherical balloons and the stress–strain ralationship was determined from the radius–pressure relationship of the balloons. In the spherical geometry, the stress is

*Author for correspondence; e-mail:
ralf.stannarius@physik.uni-magdeburg.de

Liquid Crystals ISSN 0267-8292 print/ISSN 1366-5855 online © 2004 Taylor & Francis Ltd
http://www.tandf.co.uk/journals
DOI: 10.1080/02678290410001709239

isotropic in the film plane, and because of the incompressibility of the elastomer material, an inflation of the balloon must be connected with a contraction of the smectic film normal to the surface. If the layer compression modulus in these LCE materials is comparable to that of ordinary low molar mass smectics [38], LCE balloons should show different elastic behaviour in the isotropic and smectic phases. Contrary to this expectation however, it has been found that the elastic response of such balloons is almost identical in both phases. This suggests that the smectic layer compression modulus in these samples is probably negligible with respect to the entropy elastic moduli. The material behaves qualitatively differently from the elastomers studied elsewhere [27–29]. However, the spherical geometry of the balloons is unfavourable for quantitative microscopic investigations of the elastomer films. In this work, we have solved the problem of the preparation of thin planar strips of free-standing elastomer foils of the same material. This allows us to study the samples in a geometry comparable to that in ref. [27]. The strips of ordered smectic LCE are exposed to uniaxial stress, and the in-plane deformations of the smectic films are monitored by means of optical microscopy, while the local thickness changes of the films are extracted from interference measurements. This enables us to determine the three-dimensional deformations of ordered elastomer films under uniaxial stress.

2. Experimental

2.1. *Samples*

Two types of samples are compared in this study. Materials of the first type, which will be referred to as 'diluted systems', have been studied earlier [31–34]. The synthesis of the precursor polymers has been described in detail elsewhere [31]. The random side chain copolymers consist of a siloxane backbone with attached mesogenic groups and crosslinker units (figure 1), with the substituents statistically distributed on the siloxane main chain (≈30 units). The ratio of non-substituted, mesogen-substituted and crosslinker-substituted backbone units is 2.7:(1-X):X, where crosslinker fraction X is of the order of a few percent of the total number of substituents. The structure of the crosslinker substituent has significant influence on the formation of the elastomer network. It has been shown that the siloxane backbone and the mesogenic substituents in the smectic mesophases are segregated and the backbone is essentially sandwiched between adjacent mesogen layers [39, 40]. If the length of the crosslinker unit is comparable to that of the mesogens, a three-dimensional network can form. For this network topology, the term *interlayer* crosslinked elastomer has been coined. The phase sequences of the parent polymers are given in the table.

The second type of material, referred to as 'homopolymer', consists of a fully substituted siloxane backbone with the same substituents as the 'diluted' polymers (figure 1); 7% of the mesogenic side chains carry a photoreactive end group. The phase sequence of the homopolymer is also given in the table.

2.2. *Film preparation*

The free-standing smectic films are prepared on a metal frame with three fixed edges and one movable edge, as shown in figure 2. The frame is mounted on the heating block of a Linkam TMS 600 heating stage

Table. Composition and phase transition/temperatures (°C) of the basic polymer materials.

Material	X	Y	SmX–SmC*	SmC*–SmA	SmA–I
Inter3/05	0.05	2.7	65	95–96	125
Inter3/10	0.10	2.7	45	102–104	138–140
Hom3/07	0.07	0.0	88	166	199

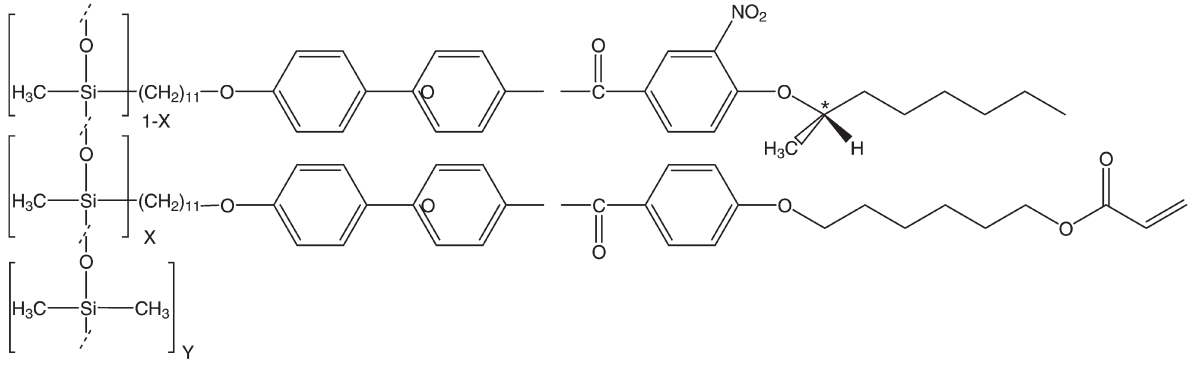

Figure 1. Chemical structure of the investigated polymers. The sample compositions (X, Y) are given in the table. For the 'diluted' polymers, $Y=2.7$, crosslinker contents are between $X=0.05$ and $X=0.15$. For the 'homopolymer', $Y=0$ and $X=0.07$.

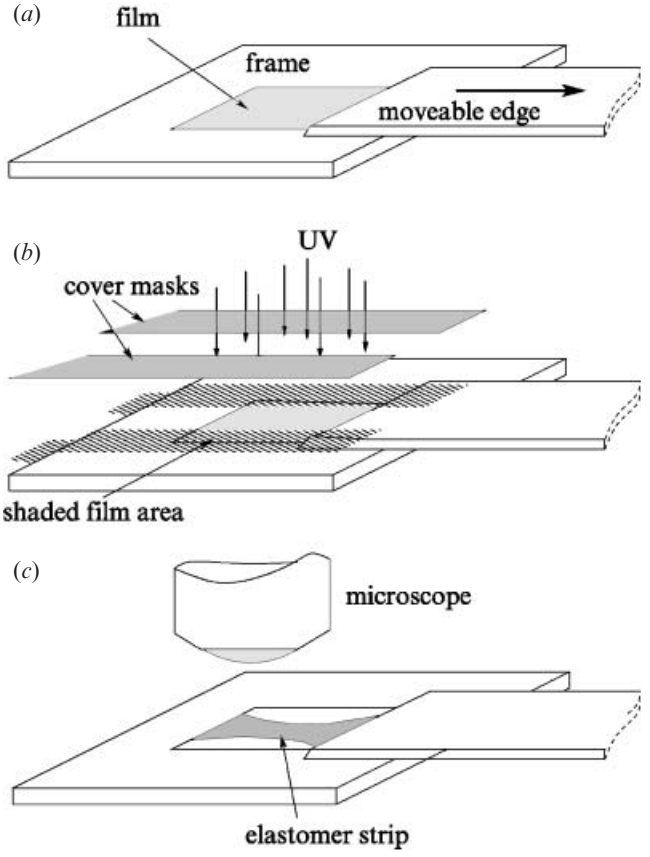

Figure 2. The three-step film preparation process. (*a*) The polymer film is drawn in the isotropic phase on a frame with three fixed edges and a movable wedge. The film area is between $\approx 1 \times 3\,\mathrm{mm}^2$ and $\approx 3 \times 3\,\mathrm{mm}^2$. After drawing, the film is annealed for at least 30 min at a temperature in the smectic A phase. (*b*) The film is irradiated with UV while its side edges are shielded from UV exposure. (*c*) The non-crosslinked material in the shaded area is removed and an elastomer strip for elastic stretch measurements remains.

for temperature control. A three-step procedure is employed to produce ordered elastomer samples: first, the movable edge is positioned close to the opposite fixed frame edge, and a small amount of smectic material is brought onto the narrow gap. This edge is then slowly drawn away by means of a microscrew, and it opens the film area, figure 2 (*a*). This step is preferentially performed in the isotropic phase where the viscosity of the material is low [33]. Both the amount of material spread initially on the frame and the drawing speed influence the resulting film thickness in a predictable way, but a controlled preparation of films with well defined thickness is not possible. One can produce films within certain thickness ranges, the film thickness varies locally.

When a sufficiently large film area has been created, the material is cooled to a temperature slightly below the isotropic–smectic A transition. In all the polymer materials studied here, the phase transition occurs across a temperature range of approximately 5 K. The formation of the smectic layers can be directly observed in the microscope images. Whereas in the isotropic phase, the films have a continuous thickness profile, and the film thickness varies smoothly (on a scale of $\approx 100\,\mu\mathrm{m}$), the smectic films have a layered structure with the layer planes stacked parallel to the film surfaces. Consequently, domains with a well defined number of smectic layers, 'terraces', are formed. These terraces are homogeneous in thickness and each shows a uniform interference colour, figure 3. These domains are usually separated by sharp, discrete thickness steps of a height of one or multiple smectic layers. During the phase transition, the remaining isotropic material collects between the smectic domains, forming circular inclusions of macroscopic dimensions 'droplets' [41]. This droplet formation is the unambiguous indication of the phase transition in the film. After the film is held for a sufficiently long time (>10 min) in the smectic temperature range, the isotropic droplets disappear completely and the film consists of ordered smectic layers in the film plane. This state is the precondition for the preparation of oriented elastomer films.

The second step is the photoreaction by UV irradiation. In order to obtain elastomer samples, we illuminate the films for approximately 20–30 min with a 200 W UV lamp. During the crosslinking process, the film profile is preserved, and individual domains in the film keep their shapes. This is an indication that the general smectic structure is not influenced by the chemical reaction, and the ordered layer structure survives. X-ray diffraction measurements of native and crosslinked films have confirmed this conclusion [33, 34].

Since we are interested in narrow elastomer strips that are attached only at two opposite edges, it is necessary to detach the elastomer films from the lateral edges of the frame. However, it is almost impossible to cut the crosslinked material from the edges of the holder without destroying the micrometer thick films. Therefore, the preparation of elastomer strips involves a slight modification of the crosslinking step, figure 2 (*b*). During UV exposure, small film areas along the side edges (a few hundred micrometers) are shielded from direct UV irradiation by opaque masks above the film. Thus, the regions near the side edges are not crosslinked, or at least are only incompletely crosslinked. The edge between the UV-exposed (elastomer) part of the films and the shielded (liquid) region can be clearly distinguished in the microscope, it is only

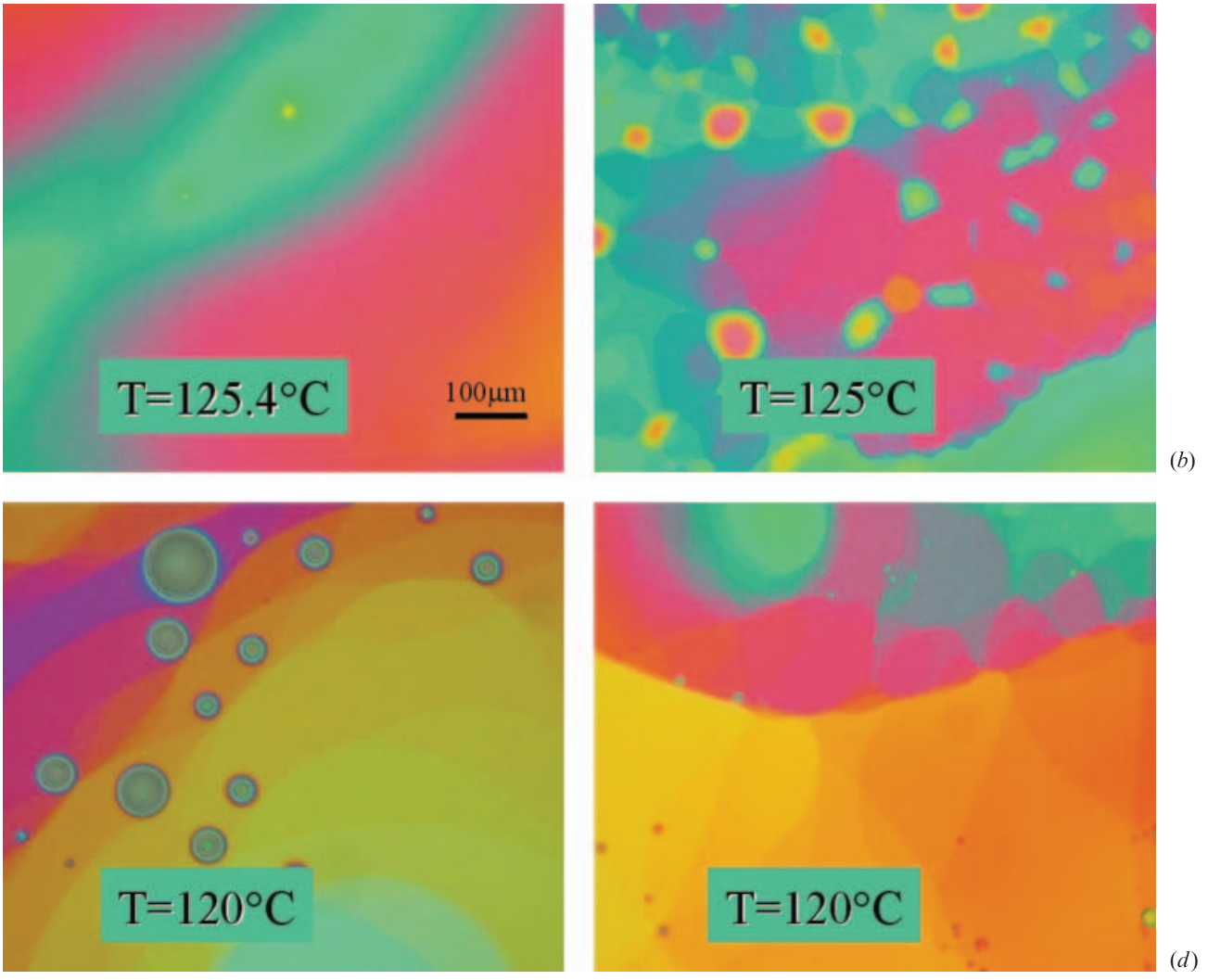

Figure 3. Change of the polymer film texture from a smooth, continuous thickness profile (*a*) in the isotropic phase through the plateau and droplet formation during the transition (*b*, *c*) to the layered smectic film with terraces (*d*). Image (*d*) was taken after the film had completely become smectic A. The film thickness ranges between ≈250 nm (light yellow region) to ≈410 nm (deep cyan region); the difference between the thickest and thinnest terraces is approximately thirty molecular layers. The image sizes are $770 \times 640\,\mu m$.

10–50 µm broad. The terrace texture is not interrupted between the two film parts. After crosslinking, the optical thickness of the films ($n \cdot d$, see next section) is smaller in the elastomer than in other parts of the film. This is probably caused by a combined effect of the shrinkage of the smectic layer spacing during crosslinking (such an effect was earlier observed in X-ray reflectivity data [34]) and a slight change of the refractive index during the chemical reaction. For the mechanical experiments performed here, this effect is not important and will not be analysed further.

The third step is the stretching of the elastomer strip by lateral displacement of the movable edge. The elastomer part of the film is reversibly deformed. In most cases, the liquid parts at the side edges of the frame rupture and leave a freely suspended elastomer strip in the middle of the frame, schematically shown in figure 2 (*c*). Sometimes, the liquid parts of the films remain intact and respond to changes of the frame area by flow. Thereby, the domain texture of the liquid part changes irreversibly, which makes liquid and elastomer parts clearly distinguishable in the microscope.

All elastic measurements of the films are performed in the smectic A phase. The reflection images are taken with a Nikon Coolpix 990 CCD camera mounted on an Axiotech polarizing microscope (Zeiss), they are further processed digitally with standard software (IDL).

2.3. *Optics*

In white light, submicrometer films show intense interference colours (see figures 3 and 4) that can be used to estimate the film thickness with an accuracy of about 10 nm. For a *quantitative* analysis of the film thickness, however, we record reflection images with four different metal interference filters (blue 488 m, green 551 nm, yellow 590 nm and red 633 nm).

Interference of light reflected at the top surface of the film with the light reflected at the bottom film surface and multiply reflected beams leads to a wavelength-dependent reflectivity $R(\lambda)$ in monochromatic light of wavelength λ

$$R(\lambda)=\frac{4\rho^2\Big/(1-\rho^2)^2\sin^2\varphi}{1+4\rho^2\Big/(1-\rho^2)^2\sin^2\varphi},\ \varphi=2\pi n_0\frac{d}{\lambda},$$

$$\text{with } \rho=\frac{n_0-1}{n_0+1}. \tag{1}$$

In the isotropic phase, the quantity n in this equation is the refractive index, and in the smectic A phase it corresponds to the ordinary refractive index. If the

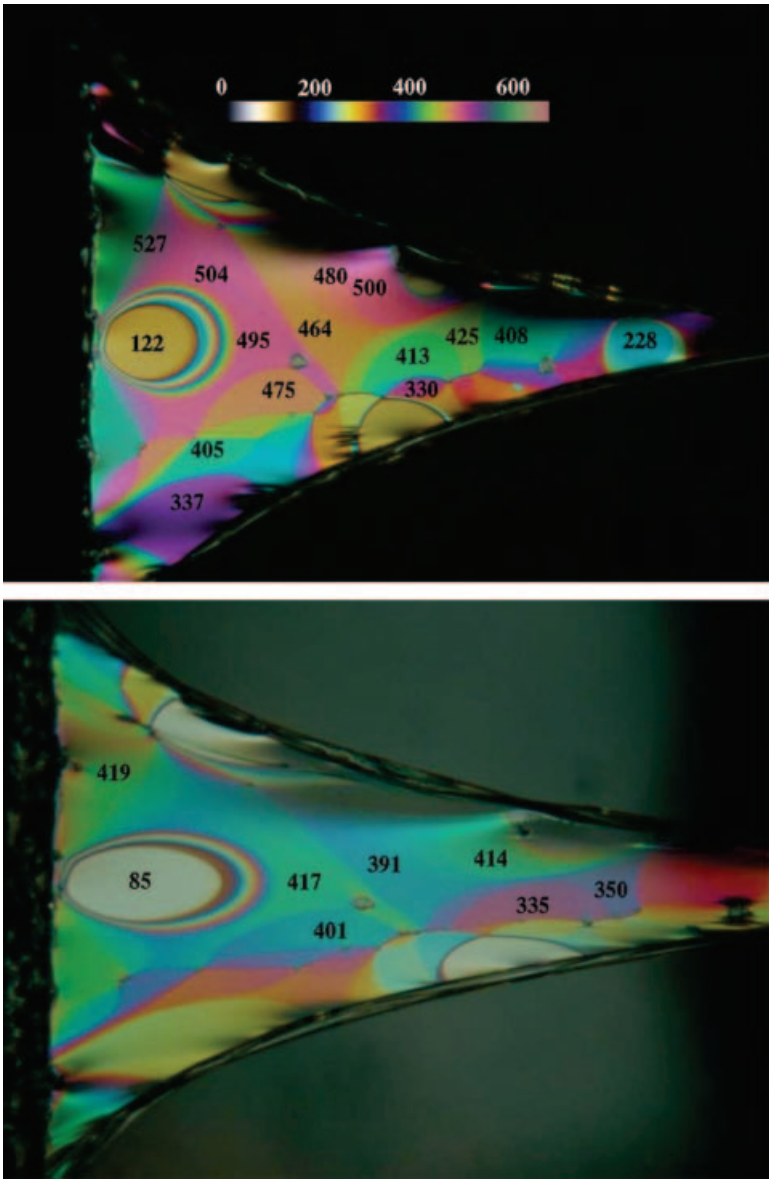

Figure 4. Inter3/05 film with thickness between ≈120 and ≈550 nm in the relaxed state (*a*) and after uniaxial stretching by 50% (*b*). Only part (≈1/2) of the films is shown, the region near the fixed edge. Image sizes are 1.17×0.88 mm. The figures on the film indicate the local film thickness in the individual domains in nm. The colour bar at the top of (*a*) visualizes the film thickness dependence of the reflection colour for an assumed refractive index $n=1.5$ (film thickness in nm).

material is cooled into the tilted smectic C* phase, or if a tilt is induced during the stretching of the film, the effective refractive index depends also upon the direction of the polarization plane of incident light with respect to the tilt plane. In the phase range studied here, this effect can be neglected and the ordinary refractive index can be used as a reasonable approximation.

The colour bar in the inset of figure 4 (*a*) gives an impression of the interference colours of films with a refractive index $n=1.5$. This colour scale helps in estimating the local film thickness from the reflection colour under white light illumination. For the construction of the map, the film reflectivities for the complete optical spectrum have been calculated, and the red, green and blue channel intensities for the RGB presentation in the digital image have been derived from the convolution of the wavelength-dependent reflectivities $R(\lambda)$ with the sensitivity curves of the three types of cone of the human eye. This approach provides a good approximation of the actual reflection colours. For the exact quantitative evaluation of film thicknesses from equation (1), however, we have referred to monochromatic images.

3. Experiment and results

The first experiment was performed with the 'diluted' elastomer. Figure 4 (*a*) shows an elastomer strip of the material Inter3/05 in the smectic A phase at 90°C. After the connections to the lateral frame edges are torn, the free boundaries of the film roll up until an arched boundary is adopted that constitutes an equilibrium of elastic forces and surface tension. In the image, only one half of the total film area is shown, the region near the fixed frame edge at the left. The film is between $\approx$120 and $\approx$550 nm thick, and the local regions of uniform film thickness are on average 100 µm in diameter. Inside these domains, the film thickness is constant to within one smectic layer ($\approx$5 nm [34]). The figures inside the domains give the local film thickness with an absolute accuracy of approximately ± 3 nm, determined from monochromic images (cf. figure 5).

Figure 4 (*b*) shows the same film region after it has been stretched (along the horizontal *x*-axis in the image) by 50%. One finds that the distortion of the domains is locally, to a good approximation, an affine transformation. A qualitatively similar observation has been reported earlier by Brodowsky *et al.* [23]. The authors of that study have focused attention on the film surface roughness and domain shapes and have disregarded a quantitative evaluation of film thicknesses.

Most interesting in figure 4 (*b*) is the dramatic colour change inside each domain as a consequence of the film contraction normal to the smectic layers. This is even more evident in the monochromatic images of figure 5 (*a*) and 5 (*b*), from the change of interference order. After an evaluation of the local film thicknesses, one finds that the film contracts, like an ordinary isotropic rubber, both in the smectic layer plane normal to the stress axis and perpendicular to the layers. The contraction is proportional to the uniaxial stretching factor. A quantitative evaluation of film thickness profiles is shown in figures 6 and 7. The film consists of the same material, Inter3/05. Figure 6 (*a*) shows a detail of the relaxed elastomer strip, and figure 6 (*b*) is the same film region, expanded along the horizontal axis to 167% of its initial length $\ell_0 = 2.5$ mm. The images have been taken with monochromatic blue illumination.

In figure 7 (*a*), examples of cross-sections of the reflectivity profiles are shown, taken along the vertical lines indicated in figures 6 (*a*) and 6 (*b*) (*y*-direction), normal to the stretching *x*-axis. These two cuts represent physically the same film material before and after stretching. In order to compare these profiles directly, the intensity curve of the stretched film has been uniformly lengthened so that the two graphs have the same size, the stretching factor of 1.29 accounts for a lateral contraction of the film along that cross-section by $-22.5 \pm 1\%$. It is clear that the local interference order of the stretched film differs considerably from that of the relaxed film. From the reflectivity curves and equation (1) one can extract the absolute thickness profiles $d(y)$. The ambiguity associated with the sine function in equation (1) can be resolved with a second reflection profile recorded with another wavelength. Figure 7 (*b*) shows the calculated local thicknesses. Again, the abscissa of the stretched film curve has been expanded by the factor 1.29 so that the two thickness profiles are directly comparable. From the profiles one can conclude that the contraction of the film perpendicular to the smectic layer planes (*z*-direction) is of the same order of magnitude as the lateral contraction of the film, the average contraction is $(-27 \pm 5)\%$. If we assume incompressibility of the material, the product $\gamma = (1+\delta x/x)(1+\delta y/y)(1+\delta z/z)$ should be invariant under stress. With the values given, one obtains $\gamma = V/V_0 = 0.945 \pm 0.1$ as an estimate for the volume ratio of stretched vs. relaxed film at a strain of 67%. This value is somewhat low but, within the accuracy of the experimental data, is consistent with the incompressibility assumption. One source of uncertainty is the assumption that the film expands uniformly in the *xy*-plane. Indeed, this assumption is exact only within regions of constant film thickness, and far away from the drawing edges. A close inspection of the profile in figure 7 (*b*) shows that the contraction factor $\delta z/z$ in the thicker film region is systematically smaller than in the thinner region, the difference is up to 20% of $\delta z/z$.

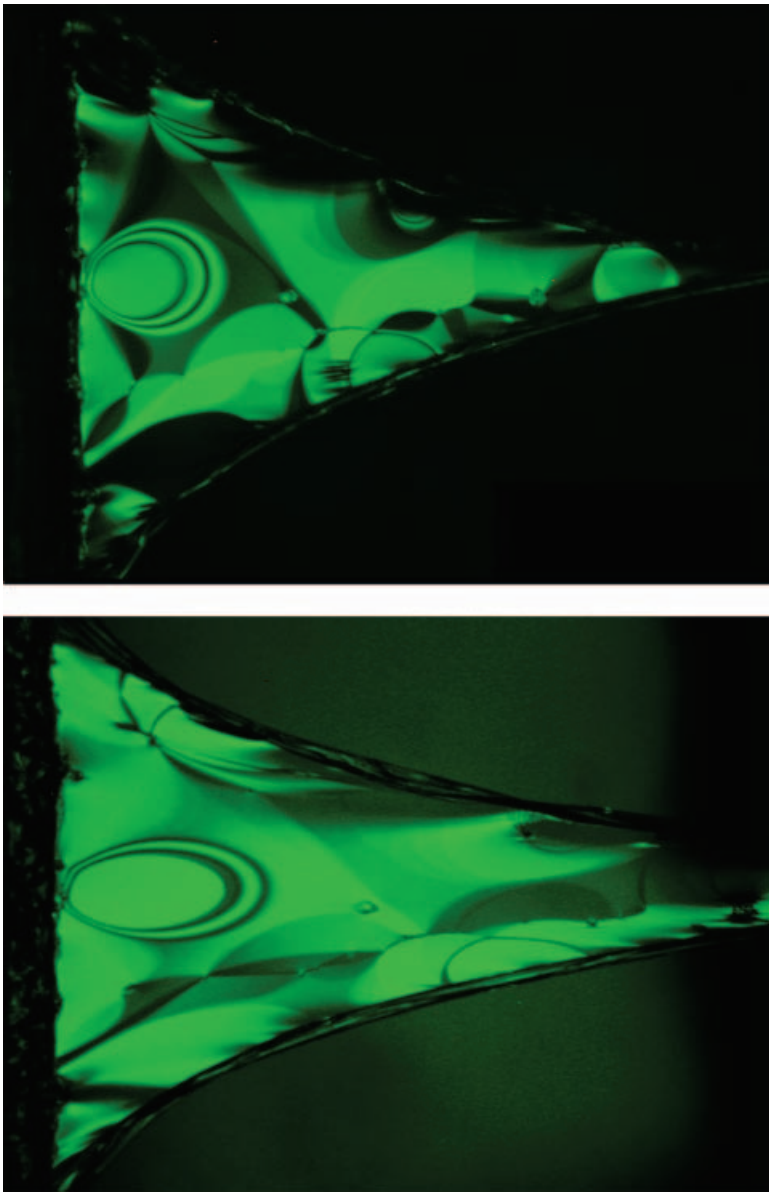

(*a*)

(*b*)

Figure 5. Same images as in figures 4 (*a*) and 4 (*b*) under monochromatic green illumination.

Figure 8 shows the ratio of the lateral contraction $\delta y/y$ vs. strain in the x-direction, determined for two films. Open squares correspond to the film shown in figure 4, circles are obtained for another film, composed of the diluted elastomer Inter3/10. Both graphs coincide qualitatively as well as quantitatively. If one assumes that the material behaves like an isotropic rubber with Poisson ratio 0.5 ($V = const$, $\delta y/y = \delta z/z$), then $\delta y/y$ should be related to $\delta x/x$ by

$$\frac{\delta y}{y} = \left(1 + \frac{\delta x}{x}\right)^{-\frac{1}{2}} - 1$$

(solid curve in the figure 8). Such a model describes the experimental data satisfactorily.

When the stress is released, the deformations are fully reversible and the sample relaxes into the initial state, cf. figure 6 (*a*). This is an indication that the smectic layer structure has not changed during the application of mechanical stress. Therefore it is reasonable to assume that the contraction of the elastomer films is related to a contraction of the smectic layer structure itself. We note that the contraction of the films normal to the smectic layer planes is in clear contrast to the observations of Finkelmann *et al.* [27] in structurally different types of smectic elastomers.

The smectic elastomer material can achieve a contraction of the molecular layers either by an interdigitation of adjacent layers, or by the induction

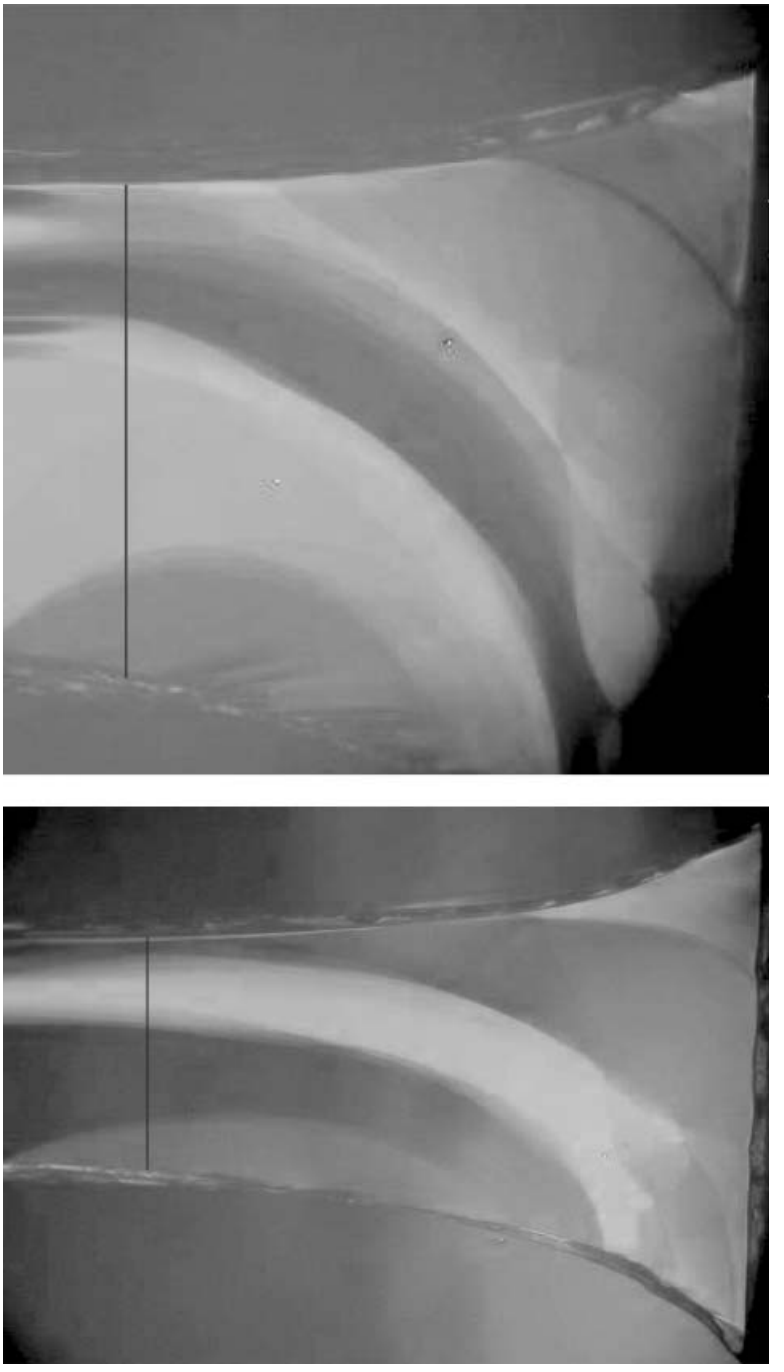

(*a*)

(*b*)

Figure 6. (*a*) Strip of an Inter3/05 film between two parallel edges with initial distance $\ell_0 = 2.5$ mm in the relaxed state, observed in blue light ($\lambda = 488$ nm). The initial film thickness is between 170 and 400 nm. (*b*) The same film after uniaxial expansion by 67%. The image sizes are (*a*) 1.26×1.25 mm (*a*) and (*b*) 1.62×1.49 mm.

of a tilt of the mesogens in the layers (transition into a smectic C* state). The latter effect may become important only when the strain is very large. For small strain, induction of a mesogenic tilt is not efficient since the layer thickness depends on the cosine of the tilt angle. In low molar mass smectics, Ribotta *et al.* have observed such an induced smectic A–smectic C transition when stress exceeding some threshold value is applied normal to the layers [42].

In the experiment, one may detect an induced tilt, at least qualitatively, from transmission microscope images. When the sample is placed between crossed polarizers,

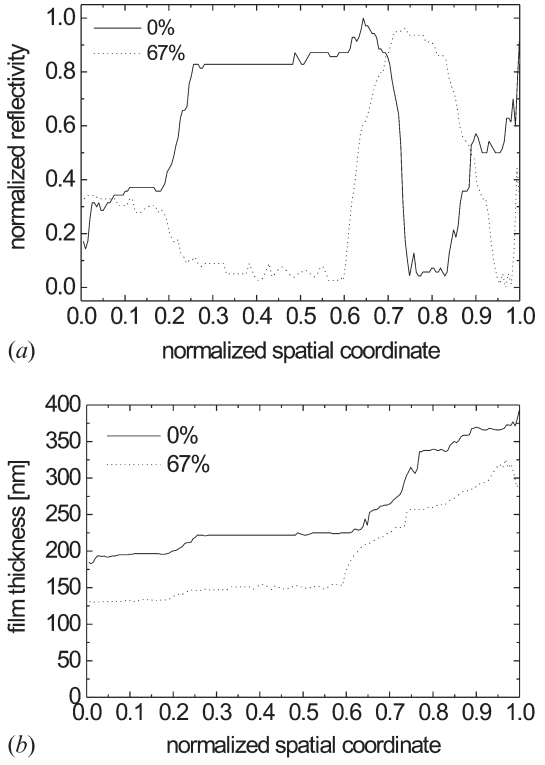

Figure 7. (*a*) Intensity profiles along the vertical cross-sections indicated in figure 6. The length of the cross-sections is 0.795 mm for the relaxed film and 0.615 mm after stretching. (*b*) Film thickness profiles along the vertical lines in figure 6, extracted from the intensity profiles (*a*), see text.

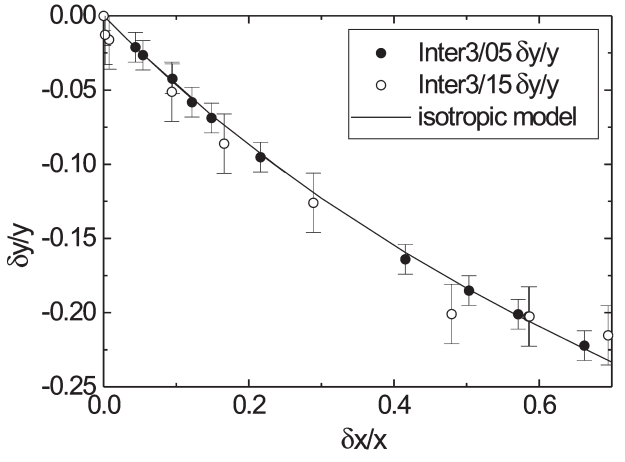

Figure 8. Plot of the lateral contraction $\delta y/y$ vs. expansion $\delta x/x$ for Inter3/05 and Inter3/10. The line is obtained under the assumption $1+\delta y/y = 1+\delta z/z = (1+\delta x/x)^{-1/2}$.

non-tilted smectic A films appear black since the optic axis is along the propagation direction of the normally incident transmitted light. If a mesogenic tilt is induced, interference of ordinary and extraordinary beams in the analyser brightens the transmission image in domains where the tilt plane is diagonal to the polarizers. A strain-induced tilt in the films is expected to be in the direction of the stretched x-axis. If one compares transmission images taken with crossed polarizers, first with the polarizers parallel and perpendicular to the stretching axis and then with polarizers diagonal to that axis, an induced tilt would manifest in a difference of the transmission intensites, which increases with larger strain. Indeed, a small birefringence of the stretched films is detected in the experiment even at very small strain (of only a few%), but it is much lower (at least one order of magnitude) than the birefringence of the native polymer films when they are cooled into the smectic C* phase. A possible induced tilt must be considerably lower than 10°. Its dependence upon the film strain is weak. Most probably, the induced small birefringence has another origin rather than an induced tilt, such as being caused by an induced anisotropy of the elastomer network. It cannnot be ruled out that the induced tilt is zero even at 70% strain. There seems to be no contribution of a mechanically induced tilt to the smectic layer contraction. One has to conclude that the smectic layer compression modulus B is very low in the diluted elastomers (cf. the value of 10.3 MPa for the materials studied in [27], which is much larger than the entropy elastic moduli in these materials). If one compares the free energy terms involved one can estimate that in the diluted elastomer samples, B must be significantly smaller than 1 MPa, the order of magnitude of the entropy elastic moduli [31, 33]. An explanation could be the large space occupied by the segregated siloxane backbone in the diluted elastomers. This non-mesogenic backbone may respond 'softly' to layer compressions.

The experiments were therefore repeated with a homopolymer that consists of the identical backbone and substituents as the diluted systems. In these systems, the mesogenic part of the layer structure is much larger, and a higher layer compression modulus can be expected. Regarding the polymeric structure, these systems correspond much more to the systems investigated by Finkelmann and coworkers, which are also homopolymers. The sample preparation is equivalent to the procedure described previously. The films prepared from the homopolymers proved to be less robust than the diluted elastomers. Nevertheless, strains up to 25% have been achieved. Figure 9 shows a section of a Hom3/07 film in the relaxed state and expanded by 23% along the x-axis (horizontal coordinate in the image). The image shows that the interference colours of the terraces, as sensitive indicators of film thickness changes, have not altered; the film has kept its thickness. Likewise, the contraction in the y-direction

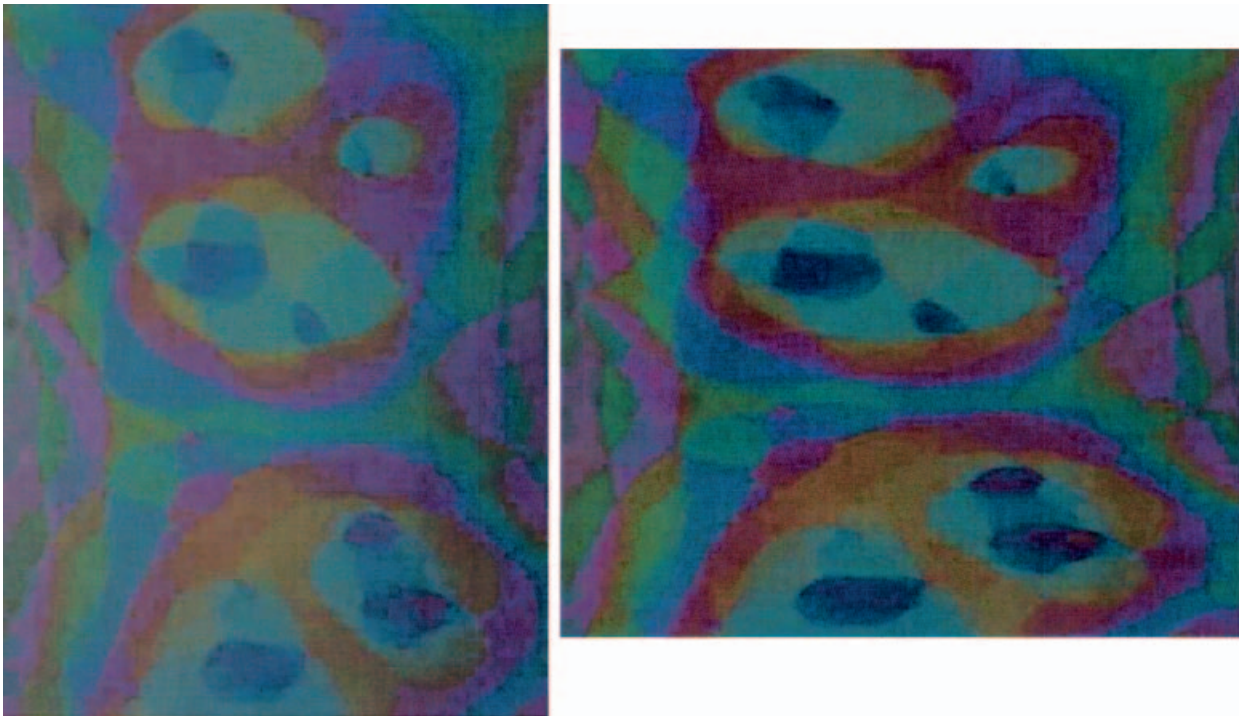

Figure 9. Images of a texture detail of the homopolymer film in white light: relaxed state (left) and the same area stretched along the x-axis (horizontal coordinate in the image) by 23% (right). In the central part, the film thickness varies approximately between 200 and 400 nm. Note that the reflectivity colours have not changed in the deformed material. Image sizes 0.38×0.47 mm (left), 0.50×0.41 mm (right).

by -17.5% fully compensates the strain in x, the ratio of the film area before and after stretching is:

$$(1+\delta x/x)(1+\delta y/y) = 0.985 \pm 0.025$$

The dependence of $\delta y/y$ on $\delta x/x$ is directly extracted from reflection microscope images. Data shown in figure 10 correspond to a sequence of images of the film region shown in figure 9. The dashed line of the isotropic model (cf. figure 8) is shown for comparison. The solid line is calculated under the assumption $\delta z = 0$ (layer incompressibility) and $(1+\delta y/y)(1+\delta x/x) = 1$ (volume incompressibility). The agreement of the latter model with the experimental data is excellent. Moreover, the evaluation of the optical interference profiles shows that the relative contraction of the films in the z-direction is at least one order of magnitude lower than the strain in the x-direction, $|\delta z'/z| < 0.02$. These results may be understood if one assumes that the smectic layer compression modulus of the investigated homopolymer is large compared with the entropy elastic contributions.

4. Conclusions and summary

Experiments with two types of smectic elastomers have shown that, depending upon the chemical composition of the elastomer, two qualitatively different deformation characteristics can be found. The diluted material with a large siloxane content behaves similarly to classical isotropic rubbers under uniaxial stress. We explain this in terms of an extraordinarily low smectic

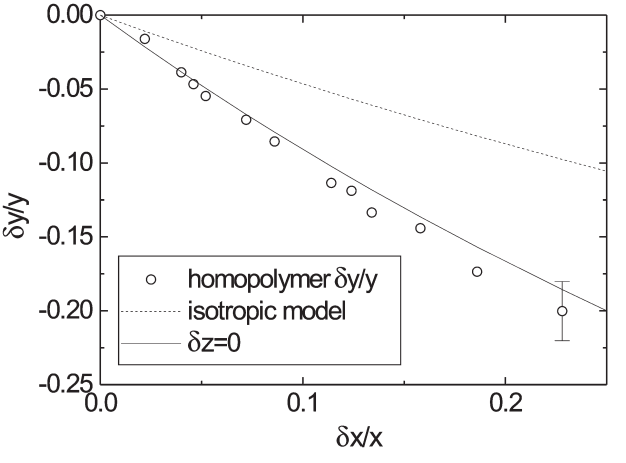

Figure 10. Plot of the lateral contraction $\delta y/y$ vs. expansion $\delta x/x$ for the homopolymer Hom3/07. The data have been extracted from the stretching factors in the area shown in figure 9. The dashed line is obtained under the assumption of incompressibility and $\delta y/y = \delta z/z$; the solid line represents the model of incompressible layers, $\delta z = 0$.

layer compression modulus. Its contribution can be neglected when the response to uniaxial strain in the smectic layer plane is described. In contrast, the homopolymer with the same mesogenic units but a fully substituted main chain behaves similarly to the materials studied in [27]. Its contraction in the direction normal to the smectic layers is very small and can be neglected for uniaxial strain in the layer plane at least up to 25%. The expansion along the stress axis is fully compensated by a lateral in-plane contraction of the ordered smectic elastomer.

From these experimental results, one can draw further conclusions on the interpretation of earlier mechanical experiments with diluted polymers. If the layer compression modulus is extremely low as a consequence of the dilution and large non-mesogenic siloxane content, one can easily understand why the measurement of the pressure vs. balloon radius in [31–33] gave similar results in the isotropic and smectic phases. Qualitatively, a change of the film thickness of smectic elastomer balloons during inflation has been reported earlier [33].

Recent investigations by Rössle *et al.* [43] gave evidence that the smectic A phase of the diluted polymer material investigated here is of a de Vries type, i.e. the mean tilt of the mesogen units with respect to the layer normal is not zero in the smectic A phase, but the tilt azimuth is not correlated in adjacent smectic layers. This lack of correlation causes an optically uniaxial appearance with macroscopic symmetry D_{∞}^{h}. It is reasonable to assume that such a phase can form in a material where neighbouring mesogen layers are separated by non-mesogenic siloxane layers, formed by the polymer backbone. This model can explain many of the mechanical features observed here. Specifically, since the molecular tilt in a de Vries material hardly changes from the smectic A to the smectic C* phase, there is no noticeable change in film area or film thickness at the phase transition. Such a change, which would be expected for a normal smectic A material, has not been found in the experiments. The model also explains the easy compressibility of the layers. A slight change of the molecular tilt may cause the layer thickness change when the film is stretched. Whereas in an ordinary smectic A phase, the layer thickness change by an induced tilt is only a second order effect, it becomes first order when the preferential molecular axis is already pretilted. Since the tilt azimuth is random, this induced tilt is not reflected in an optical birefringence in the film plane.

Irrespective of this structural model, the ultimate goal would be a direct measurement of the layer compression modulus. For low molar mass smectic materials, no direct measurement of the static modulus exists. The problem of such measurements is the fluidity of the material. Data of the dynamic modulus can be obtained, for example from dynamic vibration analysis [42–44, 45] or ultrasound measurements [46, 47]. The storage moduli for low molar mass smectogens are in the range of several MPa in the smectic A phase [48]. In the elastomers, the situation may be somewhat easier, since problems connected with macroscopic flow during the measurements are avoided. The direct approach chosen by Finkelmann and coworkers [27] is best adapted to the problem. However, due to the very different preparation methods of the ordered elastomer samples, it is not applicable to the materials studied here.

The authors acknowledge financial support by the DFG within grant Sta 425/14.

References

[1] Gleim, W., and Finkelmann, H., 1989, in *Side Chain Liquid Crystalline Polymers*, edited by C. B. McArdle (Glasgow: Blackie); Finkelmann H., 1991, in *Liquid Crystallinity in Polymers*, edited by A. Ciferri (Weinheim: VCH).

[2] Zentel, R., 1989, *Angew. Chem. adv. Mater.*, **101,** 1437.

[3] Davis, F. J. J., 1993, *Mater. Chem.*, **3,** 551.

[4] Kelly, S. M., 1998, *Liq. Cryst.*, **24,** 71.

[5] Terentjev, E. M., 1999, *J. Phys. cond. Mat.*, **11,** R239.

[6] Wong, G. C. L., de Jeu, W. H., Shao, H., Liang, K. S., and Zentel, R., 1997, *Nature*, **389,** 576.

[7] Finkelmann, H., Nishikawa, E., Pereira, G. G., and Warner, M., 2001, *Phys. Rev. Lett.*, **87,** 015501.

[8] Clarke, S. M., Tajbakhsh, A. R., Terentjev, E. M., and Warner, M., 2001, *Phys. Rev. Lett.*, **86,** 4044.

[9] Mao, Y., and Warner, M., 2001, *Phys. Rev. Lett.*, **86,** 5309.

[10] Warner, M., Terentjev, E. M., Meyer, R. B., and Mao, Y., 2000, *Phys. Rev. Lett.*, **85,** 2320.

[11] Taheri, B., Muñoz, A. F., Palffy-Muhoray, P., and Twieg, R., 2001, *Mol. Cryst. liq. Cryst.*, **358,** 73.

[12] Finkelmann, H., Kim, S. T., Muñoz, A., Palffy-Muhoray, P., and Taheri, B., 2001, *Adv. Mater.*, **13,** 1069.

[13] Brehmer, M. *et al.*, 1994, *Macromol. Chem. Phys.*, **195,** 1891.

[14] Brehmer, M., and Zentel, R., 1995, *Macromol. Chem. rapid Commun.*, **16,** 659.

[15] Benné, I., Semmler, K., and Finkelmann, H., 1995, *Macromolecules*, **28,** 1854.

[16] Brehmer, M. *et al.*, 1996, *Liq. Cryst.*, **21,** 589.

[17] Gebhard, E., and Zentel, R., 2000, *Macromol. Chem. Phys.*, **201**, 902; Gebhardt, E., and Zentel, R., 2000, *Macromol. Chem. Phys.*, **201**, 911.

[18] Valerien, S. U. *et al.*, 1990, *Macromol. Chem. rapid Commun.*, **11,** 593.

[19] Lehmann, W., Skupin, H., Tolksdorf, C., Gebhard, E., Zentel, R., Krüger, P., Lösche, M., and Kremer, F., 2001, *Nature*, **410,** 447.

[20] Gebhard, E., and Zentel, R., 1999, *Liq. Cryst.*, **26,** 299.

[21] Shilov, S. V. *et al.*, 1997, *Liq. Cryst.*, **22,** 203.

[22] Skupin, H. *et al*., 1999, *J. macromol. Sci. Phys. B*, **38,** 709.
[23] Brodowsky, H. M. *et al*., 1999, *Langmuir*, **15,** 274.
[24] Hirschmann, H., Velasco, D., Reinecke, H., and Finkelmann, H., 1991, *J. Phys. II (Fr)*, **1,** 559.
[25] Lehmann, W. *et al*., 1998, *Ferroelectrics*, **208–209,** 373.
[26] Lehmann, W. *et al*., 2000, *Ferroelectrics*, **243,** 107.
[27] Kundler, I., Nishikawa, E., and Finkelmann, H., 1997, *Macromol. Symp.*, **117,** 11.
[28] Nishikawa, E., Finkelmann, H., and Brand, H. R., 1997, *Macromol. rapid Commun.*, **18,** 65.
[29] Nishikawa, E., 1997, PhD thesis, Freiburg, Germany.
[30] Weilepp, J., Stein, P., Assfalg, N., Finkelmann, H., Martinoty, P., and Brand, H. R., 1999, *Europhys. Lett.*, **47,** 508.
[31] Schüring, H., Stannarius, R., Tolksdorf, C., and Zentel, R., 2001, *Macromolecules*, **34,** 3962.
[32] Schüring, H., Stannarius, R., Tolksdorf, C., and Zentel, R., 2001, *Mol. Cryst. liq. Cryst.*, **364,** 305.
[33] Stannarius, R., Köhler, R., Dietrich, U., Lösche, M, Tolksdorf, C., and Zentel, R., 2002, *Phys. Rev. E*, **65,** 041 707.
[34] Köhler, R. *et al*., 2002, *Proc. SPIE*, **4759,** 483.
[35] Ortiz, C., Ober, C. K., and Kramer, E. J., 1998, *Polymer*, **39,** 3713.
[36] Roberts, P. M. S., Mitchell, G. R., and Davis, F. J., 1997, *J. Phys. II (Fr)*, **7**, 1337; Roberts, P. M. S., Mitchell, G. R., Davis, F. J. and Pople, J. A. 1997, *Mol. Cryst. liq. Cryst*., **299**, 181.
[37] Schmidt, F., Siepmann, J., Stille, W., and Strobl, G. R., 2000, *Mol. Cryst. liq. Cryst.*, **350,** 103.
[38] De Gennes, P. G., 1974, *The Physics of Liquid Crystals* (Oxford University Press), p. 286.
[39] Diele, S. *et al.*, 1987, *Macromol. Chem.*, **188,** 1993.
[40] Poths, H., and Zentel, R., 1994, *Liq. Cryst.*, **16,** 749.
[41] Schüring, H., and Stannarius, R., 2003, *Langmuir*, **18,** 9735.
[42] Ribotta, R., Meyer, R. B., and Durand, G., 1974, *J. Physique Lett.*, **35,** 161.
[43] Rössle, M., Zentel, R., Lagerwall, J., and Gießelmann, F. *Liq. Cryst*. (in the press).
[44] Ribotta, R., and Durand, G., 1977, *J. Physique*, **38,** 179.
[45] Martinoty, P., Sonntag, P., Benguigui, L., and Collin, D., 1994, *Phys. Rev. Lett.*, **73,** 2079.
[46] Brochard, F., 1974, *Phys. Lett. A*, **49,** 315.
[47] Kawamura, Y., Okano, K., and Iwayanagi, S., 1981, *Jpn. J. appl. Phys.*, **20,** L309.
[48] Martinoty, P., Gallani, J. L., and Collin, D., 1998, *Phys. Rev. Lett.* **81,** 144; Bartolino, R. and Durand, G. 1984, *Nuovo Cimento D*, ser. 1, **3D,** 903; Shibahara, S. *et al*.; 2000, *Phys. Rev. Lett*., **85,** 1670; Shibahara, S. *et al*.; 2000, *Ferroelectrics*, **244,** 459; Shibahara, S. *et al*.; 2002, *Phys. Rev. E*, **65,** 030702.